

## CHEMICAL STRUCTURES AND THEORETICAL MODELS OF LEAN PREMIXED ATMOSPHERIC-PRESSURE PROPENE/O<sub>2</sub>/N<sub>2</sub> FLAMES

A. Seydi<sup>1\*</sup>, J. Biet<sup>2</sup>, J.L. Delfau<sup>2</sup> and C. Vovelle<sup>2</sup>

<sup>1</sup>Département de Chimie, Faculté des Sciences et Techniques, Université C.A. Diop, Dakar, Sénégal

<sup>2</sup>Laboratoire de Combustion et de Systèmes Réactifs, CNRS, 45071 Orléans, France

(Received January 5, 2011; revised January 11, 2012)

**ABSTRACT.** To better understand the chemistry involved in the lean-fuel combustion, the chemical structure of lean premixed propene-oxygen-nitrogen flames stabilized on a flat-flame burner at atmospheric pressure was determined experimentally. The species mole fraction profiles were also computed by the Premix code and three detailed reaction mechanisms. A very good agreement was observed for the main properties: reactants consumption, final products (CO<sub>2</sub>, H<sub>2</sub>O) and the main intermediates: CO and H<sub>2</sub>. Only a general agreement is also observed between predicted and measured mole fraction profiles for minor intermediates. Marked differences occurred in the prediction of active intermediate species present in small concentrations. Pathways analyses were performed to identify the origins of these discrepancies. It was shown that the same reactions were involved in the three mechanisms to describe the consumption of propene, but with marked differences in their importance. C<sub>2</sub>H<sub>5</sub>, C<sub>2</sub>H<sub>4</sub>, and C<sub>3</sub>H<sub>5</sub> are the main species formed in the first step and their consumption increases the differences between the mechanisms either by the use of different kinetics data for common reactions or by differences in the nature of the consumption reactions.

**KEY WORDS:** Flame structure, Lean flame, Propene, Combustion mechanisms

### INTRODUCTION

Lean premixed combustion has been considered as one of the promising solutions for fuel economy and the reduction of pollutants emission (CO, nitric oxides, and soot). Indeed, using lean premixed flames to produce energy in gas turbine is considered as an efficient way to reduce pollutants levels in exhaust gas. Soot and poly aromatic hydrocarbons (PAH) are not formed in lean flames. CO is formed as intermediate species but readily converted into CO<sub>2</sub>. A decrease in the maximum temperature and in concentration of CH<sub>2</sub> radicals limits NO<sub>x</sub> formation to very low levels. On the other hand, very lean flames are subjected to instabilities and eventually extinction with, as potential risk, the presence of partial oxygenated species, such as aldehydes, in the exhaust gas. A better knowledge of the combustion chemistry of fuel-oxygen mixtures is needed to overcome these limitations.

The main objective of this work was to determine the structures of lean flames, and on another hand, to control the ability of combustion mechanisms to correctly predict the chemistry of very lean flames.

The analysis of the structure of premixed laminar flames is well adapted for deriving experimental data representation of combustion conditions. This technique has been applied to the study of lean premixed flames of small hydrocarbons at sub-atmospheric [1-7] or atmospheric pressure [8-11].

However, to our knowledge, no systematic experimental investigation of the influence exerted by a progressive reduction of the equivalence ratio on the structure of lean premixed flames has been carried out in atmospheric-pressure flames.

\*Corresponding author. E-mail: aseydi@ucad.sn

As started by Warnatz [12], large fuel molecules (i.e. components of gasoline, gas oil, kerosene) are decomposed very fast into small  $C_1$  and  $C_2$  fragments that are further oxidized in a reaction sequence that control kinetically the whole process.

Previous studies by our group on the lean premixed flames fed by small fuel molecules at atmospheric pressure were performed [13-14], and this work has focused on propene flames in order to complete these studies. All experiments were carried out under conditions similar to these previous studies.

Several groups have carried out both experimental and numerical studies to improve the knowledge of propene oxidation and pyrolysis [15-35]. On the whole, these studies were carried out on rich propene flames, and less studies have been devoted to lean flames, because the interest for understanding of soot,  $NO_x$  and PAH formation and/or suppression chemistry in combustion processes of the hydrocarbons. The understanding of propene oxidation is an important step in the development of chemical kinetic mechanisms for large hydrocarbon fuels. Propene is the main intermediate produced in the oxidation of many hydrocarbon fuels (octane, pentane, butane, and propane). The chemical kinetic sub-mechanism for the oxidation of propene is an important part of the overall kinetic mechanism for these fuels. With the development of premixed lean combustion to reduce pollutants production, unfortunately, no recent systematic data for the lean propene-oxygen flames are available in the literature. Therefore, there is a need for data obtained in lean atmospheric-pressure flames. In this work, the structures of lean propene-oxygen flames, diluted by nitrogen, was studied experimentally, with equivalence ratios (the fuel-to-oxygen ratio in the mixture to one in stoichiometric conditions) ranging from 0.83 to 0.48.

In addition to the experimental determination of species mole fraction profiles, the chemical structure of the flames was computed by a simulation code with three combustion mechanisms available in the literature, as input data [36-38]. A special care was taken into the examination of the relative importance of the various propene consumption pathways.

## EXPERIMENTAL

Propene-oxygen-nitrogen flames were stabilized on a flat-flame burner at atmospheric pressure. The upper part of the burner was made of a brass disc with small holes (0.7 mm diameter) drilled on a 4.0 cm diameter circular area. A perforated plate was located 1 cm above the burner surface to reduce heat exchanges between the flame and the burner and move the flame downstream. Actually, this plate played its expected role and lean propene flames reported here were stabilized 2.5 cm above the burner surface.

Table 1 lists the initial conditions for the four flames studied, in term of parameters needed for simulations with premix code. The  $N_2/O_2$  ratios were adjusted in order to improve the stability of the leanest flames or to maintain a minimum distance between the flame front and the burner surface for the richest flame ones.

Table 1. Initial conditions of the four  $C_3H_6-O_2-N_2$  flames (pressure 101 kPa).

Mole fractions	Flame 1	Flame 2	Flame 3	Flame 4
$C_3H_6$	0.0284	0.0302	0.0329	0.0323
$O_2$	0.2641	0.2220	0.1975	0.1750
$N_2$	0.7075	0.7478	0.7696	0.7930
Equivalence ratio	0.48	0.61	0.75	0.83
Mass flow rate ( $g \cdot cm^{-2} \cdot s^{-1}$ )	0.0199	0.0240	0.0283	0.0260

Gases samples were taken along the symmetry axis of the flame by a quartz microprobe, mounted on a micrometer stage for vertical adjustment of the probe position relative to the burner surface. The probe was constructed from a 0.5 cm diameter quartz tube drawn to a cone at the end. A hole (0.1 mm diameter) was drilled at the tip of this cone.

The following chemicals were used as reactants: C<sub>3</sub>H<sub>6</sub> (99.5%, with C<sub>3</sub>H<sub>8</sub> as impurities), O<sub>2</sub> (99.5%), N<sub>2</sub> (99.5%) were bough from Air Liquide Industries.

Gases samples were withdrawn from the flame through the probe and either directly injected into a gas chromatograph or stored in Pyrex sample flasks at a pressure limited to about 4 kPa to quench the chemical reactions with the hot tip of the probe.

Gases samples withdrawn from the flame were analysed either by gas chromatograph (GC) or by the Fourier transform infrared spectroscopy (FTIR). Species analysed by GC were CH<sub>4</sub>, C<sub>2</sub>H<sub>4</sub>, C<sub>2</sub>H<sub>2</sub>, C<sub>2</sub>H<sub>6</sub>, C<sub>3</sub>H<sub>6</sub>, CO, CO<sub>2</sub>, CH<sub>3</sub>CHO, H<sub>2</sub>, O<sub>2</sub>, and N<sub>2</sub>. Those measured by FTIR were CH<sub>2</sub>O, H<sub>2</sub>O, CO, and CO<sub>2</sub>.

Two GC systems were used for the analyses. The first one (Hewlet Packard HP6890) was equipped with a thermal conductivity detector (TCD) and kitted out with two capillaries columns (Porous-Layer-Open-Tubular: Poraplot) connected in series. Hydrocarbon intermediate species and carbonyl compounds were separated on the Porapak column (packed column with a porous material as a stationary phase) whereas the molecule sieve was used to separate permanent gases such as H<sub>2</sub>, O<sub>2</sub>, N<sub>2</sub>, CH<sub>4</sub>, and CO. Gases samples were flowing continuously trough the introduction loop at a pressure limited to 4 kPa. The combined effects of the use of a TDC and this low introduction pressure led to a detection limit of the order of 100ppm.

Because of their very short retention time on the Poraplot Q (a divinyl-benzene/styrene system as a stationary phase), the permanent gases entered rapidly into the molecule sieve which was isolated by a switch valve to avoid its contamination by compounds such as CO<sub>2</sub> and H<sub>2</sub>O. When all intermediate species were eluted from the Porapak column, the molecular sieve column was put back in series and the permanent gases were analysed.

The second chromatograph operated with a flame ionization detector (FID) and was used for the separation of CH<sub>4</sub> and C<sub>2</sub>-C<sub>3</sub> intermediates on an Al<sub>2</sub>O<sub>3</sub>/KCl column. Prior to its injection into a column, the gas sample collected at about 2.0-2.7 kPa was compressed at 53.0 kPa by means of a special device [39]. This compression greatly enhances the detection limit which was estimated to be about 1 ppm.

Helium was used as carrier gas for all species analyses, except H<sub>2</sub> which was measured with nitrogen to enhance the detector sensitivity.

Species calibration was performed by using a gaseous mixture of known composition. The accuracy was estimated to be  $\pm 5\%$  for the permanent gases and C<sub>1</sub> and C<sub>2</sub> hydrocarbons,  $\pm 10\%$  for C<sub>3</sub>H<sub>6</sub> and  $\pm 20\%$  for CH<sub>2</sub>O and CH<sub>3</sub>CHO.

FTIR analyses were performed with the cell filled by the sampled gases up to 3.31 kPa. The selected special windows were 2118.3-2128.8 cm<sup>-1</sup> for CO, 2379.3-2381.2 cm<sup>-1</sup> for CO<sub>2</sub>, 1716.6-1719.2 cm<sup>-1</sup> for H<sub>2</sub>O, and 1744.1-1746.7 cm<sup>-1</sup> for CH<sub>2</sub>O. For the latter, the signal had to be corrected for a contribution from H<sub>2</sub>O.

Temperature profiles were measured by using a Pt/Pt-10% Rh thermocouple made of 50- $\mu$ m-diameter wires coated with a BeO-Y<sub>2</sub>O<sub>3</sub> deposit to reduce catalytic effects [40]. Radiation losses were corrected using the classical electrical compensation technique [41]. In a first series of experiments, the thin wires on each side of the bead were only 0.5 cm long and were soldered to thicker wires (0.5 mm diameter) maintained by a ceramic capillary [39]. However, even with this capillary installed, heat conduction from the thick wires led to the experimental temperature systematically shifted toward the burner with respect to the species mole fraction profiles. A new thermocouple was constructed with thin wires 4 cm long, tightened parallel to burner surface and connected to ticker wires on the sides of the burner. The temperature profiles measured in the four flames with this new thermocouple have been plotted on Figure 1. Based

on measurement reproducibility the accuracy was estimated to 5%. To improve the flames stability, changes in the ratio  $N_2/O_2$  limit the variation of the maximum temperature to less than 200 K when the equivalence ratio was decreased from 0.9 to 0.48.

### *Modelling*

The lean flame structures were computed by using the Chemkin II [42] and Premix [43] codes. Three detailed combustion mechanisms currently available on Web sites have been used to compute the species mole fraction profiles.

UDEL [36] mechanism is based upon addition of reactions for  $C_3$  to  $C_6$  species to the GRI-mech mechanism [44]. It includes 70 species and 455 reactions.

The mechanism developed by Konnov [37] is more detailed. In its original version, it contains 127 species  $C_xH_yO_z$  from  $C_0$  to  $C_6$  and nitrogenous intermediates. These species are involved in 1158 reversible reactions and 49 non-reversible reactions. In this work, the N-species subsystem was removed so that the number of species was reduced to 93 and the number of reactions to 730 reversible and 47 non-reversible.

The third mechanism has been developed by the Combustion Division of the Centre for Energy Research at the University of California (UCSD) [38] with the objective to describe phenomena relevant to flame conditions with the number of reactions and species kept to a minimum. The 2002 version (2002-1001) has been used in this work. It contains 39 species (up to  $C_3$ ) involved in 179 reactions (167 reversible and 6 reactions with kinetic parameters given for the forward and reverse reactions).

The thermodynamic and transport data have been taken without any change from the respective Web sites.

Flames simulations were performed with the "BURN" option and experimental temperature profiles introduced as input data. They were also conducted with "FREE" option, however, as the Premix code was used, the experimental temperature profile was only an initial estimate and the final temperature profile was computed by solving the energy equation. The latter procedure led to maximum temperatures only slightly higher than the measured ones, showing that due to the care taken to stabilize each flame with an overall flow rate close to the maximum value compatible with flame stability, the four flames were almost adiabatic.

## **RESULTS AND DISCUSSION**

In both flames the temperature gradient and the burned gases temperature are very well reproduced by Konnov, UCSD, and UDEL mechanisms as shown in Figure 1. With UDEL mechanism, the slope is smaller and profile is shift away from the burner surface in the leanest flame. The very good agreement observed for the maximum temperature shows that experimental heat losses were reduced to a minimum and the flames were stabilized in adiabatic conditions.

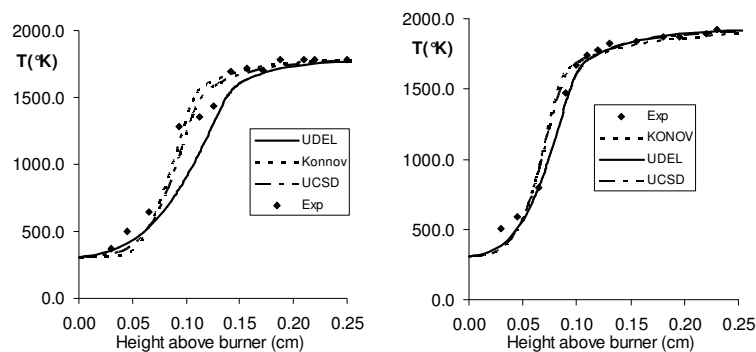


Figure 1. Computed (lines) and measured (symbols) for temperature profiles in lean ( $\Phi = 0.48$ , left;  $\Phi = 0.83$ , right) propene flames.

The experimental profiles were shifted to take account the results of species measurements performed with the sampling probe and the thermocouple simultaneously present in the flame. These measurements showed that the probe did not influence the thermocouple signal when it was (the probe) not connected to the vacuum pump. As soon as the pressure in the probe was reduced, to reproduce the sampling conditions, a marked reduction in the thermocouple signal was observed. An increase in the distance separating the probe and the thermocouple resulted in a progressive increase in the thermocouple signal up to the “unperturbed” value, measured with the probe located very far from the thermocouple. This maximum “perturbation distance” decreased when the pressure maintained in the probe was increased. It was also smaller at low temperature upstream the flame front. In order to superimpose the temperature profiles with the species ones, a shift position ( $Z'$ ) was derived from the position of the sampling probe ( $Z$ ) from the expression:

$$Z' = z - d \times \frac{T_{(z)} - T_0}{T_{\max} - T_0} \quad (1)$$

where  $T_0$  temperature at the burner surface,  $T_{\max}$  maximum flame temperature and  $d$  maximum shift distance. The latter increased when the sampling pressure decreased and the following values were used: 0.02 mm ( $GC_1$ ), 0.05 cm ( $GC_2$ ) and 0.03 cm (FTIR).

Others [45] used a different approach to that end, using molecular beam mass spectrometry in order to measure the species concentration profiles, and, instead of  $Z'$ , they computed  $T_z$ , the local temperature. In their investigations, the individual temperature profiles were superimposed with the mole fraction profile scale ( $Z$ ) by comparison with the water mole fraction profile by using equation:

$$T_z = T^\circ + [(X_{H_2O})_z / (X_{H_2O})_{\max}] (T_{\max} - T^\circ) \quad (2)$$

$T_{\max}$ ,  $T_z$ , and  $T^\circ$ , are the maximum, local and initial temperature, respectively and  $(X_{H_2O})_{\max}$  and  $(X_{H_2O})_z$ , are the maximum and local mole fraction of water.

The three mechanisms tested reproduce very well the consumption of reactants (Figure 2) and formation of main products: CO<sub>2</sub> and H<sub>2</sub>O (Figure 3). The down-stream shift noticed with UDEL mechanism for the temperature in the leanest flame leads to a similar shift in the species mole fraction profiles.

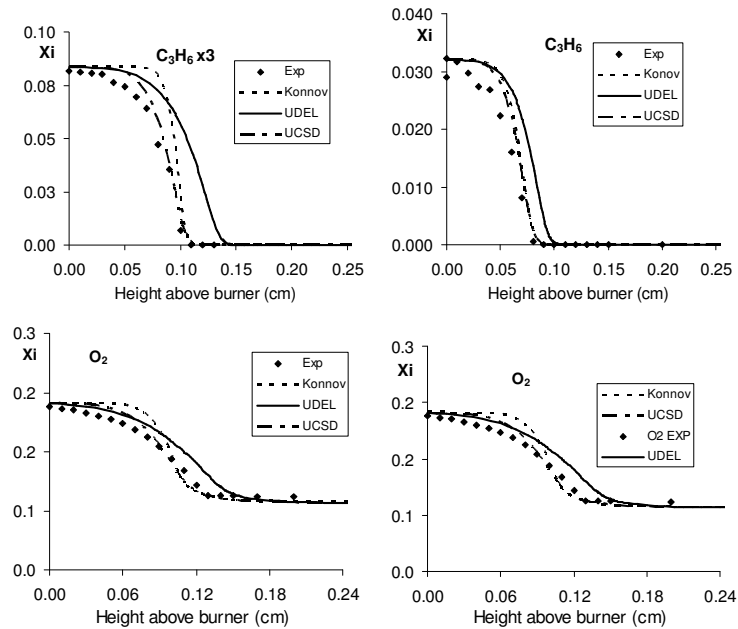


Figure 2. Computed (lines) and measured (symbols) for reactants profiles in lean ( $\Phi = 0.48$ , left;  $\Phi = 0.83$ , right) propene flames.

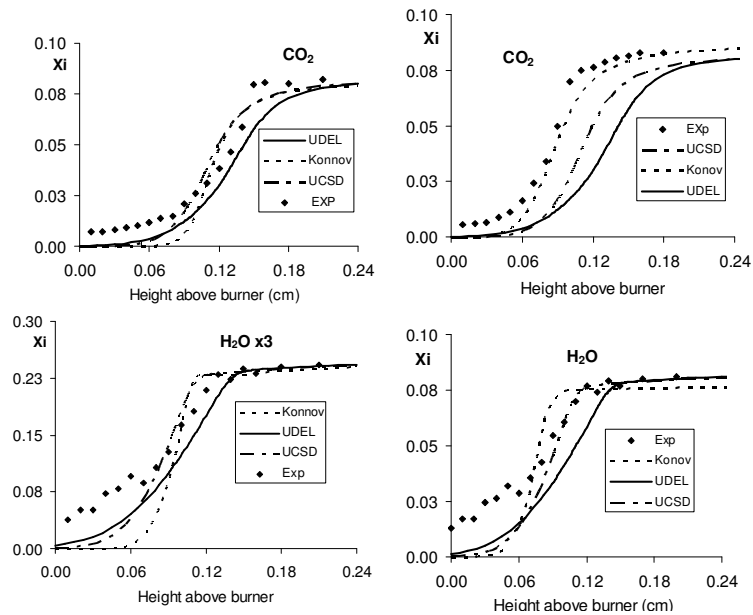


Figure 3. Computed (lines) and measured (symbols) for final products profiles in lean ( $\Phi = 0.48$ , left;  $\Phi = 0.83$ , right) propene flames.

With Konnov, UCSD mechanisms the computed profiles are almost identical and perfectly reproduce the experimental evolutions. The three mechanisms predict post-flame concentrations in very good agreement with experiments. Such a good agreement must be expected since in lean flames, CO<sub>2</sub> and H<sub>2</sub>O are the only final products corresponding to the complete conversion of carbon and hydrogen.

CO and H<sub>2</sub> are the main intermediate species in these flames. In both flames, slight differences are observed in the modelling of CO and H<sub>2</sub>, as shown in Figure 4. The computed profiles are in good agreement with the measured for CO (Figure 4). The maximum mole fraction is slightly over predicted by the models but the evolution of this maximum value with the equivalence ratio is well reproduced. Konnov and UCSD mechanisms give very close profiles, in very good agreement with experimental data for H<sub>2</sub> and they slightly over-predict CO. For H<sub>2</sub> computed profiles are markedly smoother than the experimental ones. This difference is likely to result from the diffusion term in species conservation equation.

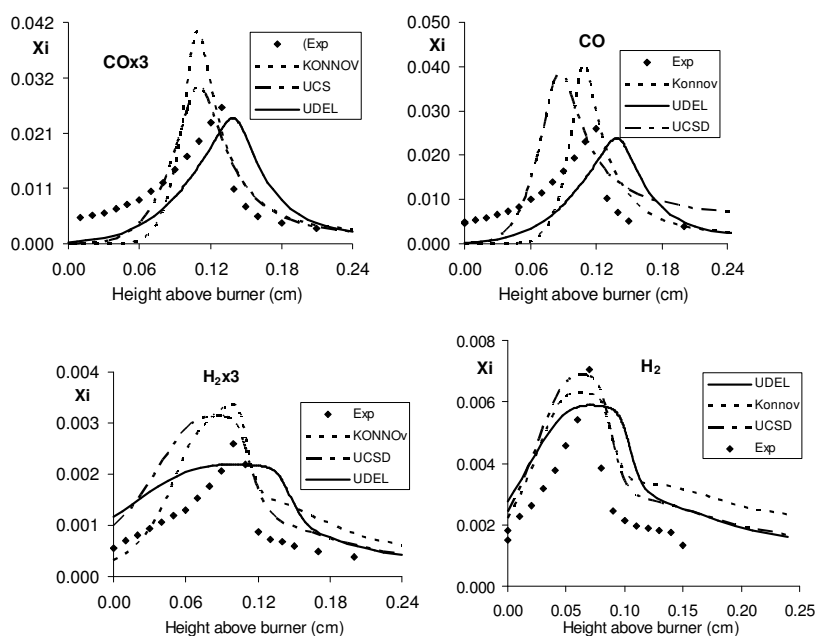


Figure 4. Computed (lines) and measured (symbols) for main intermediate species profiles in lean ( $\Phi = 0.48$ , left;  $\Phi = 0.83$ , right) propene flames.

Other intermediate species include small hydrocarbons: ethylene, acetylene, ethane, and methane (Figures 5-7). They are all consumed very fast so their mole fraction profiles have a strong negative gradients after the maximum. In the richest flame, the experimental profiles start with finite values at the burner surface showing that reaction quenching in the probe was not efficient enough. A general agreement is observed between predicted and measured mole fraction profiles Figure 6 shows that CH<sub>4</sub> is slightly over predicted in the  $\Phi = 0.48$  flame by Konnov mechanism and under predicted by the three mechanisms in the  $\Phi = 0.83$ . For C<sub>2</sub>H<sub>6</sub>, in the  $\Phi = 0.48$  flame, Konnov mechanism over predicts whereas UDEL and UCSD mechanisms under predict, but in the  $\Phi = 0.83$  UDEL reproduces very well the maximum mole fraction. The

modelling of  $C_2H_2$  exhibits marked differences between Konnov and the two others (Figure 5). In the leanest flame, the former markedly over predicts the maximum mole fraction, whereas in the richest flame, it reproduces fairly well the experimental data. For  $C_2H_4$  mole fraction profile, Konnov mechanism over predicts in both flames and the two others mechanisms product similar profiles with maximum value fairly well reproduced.

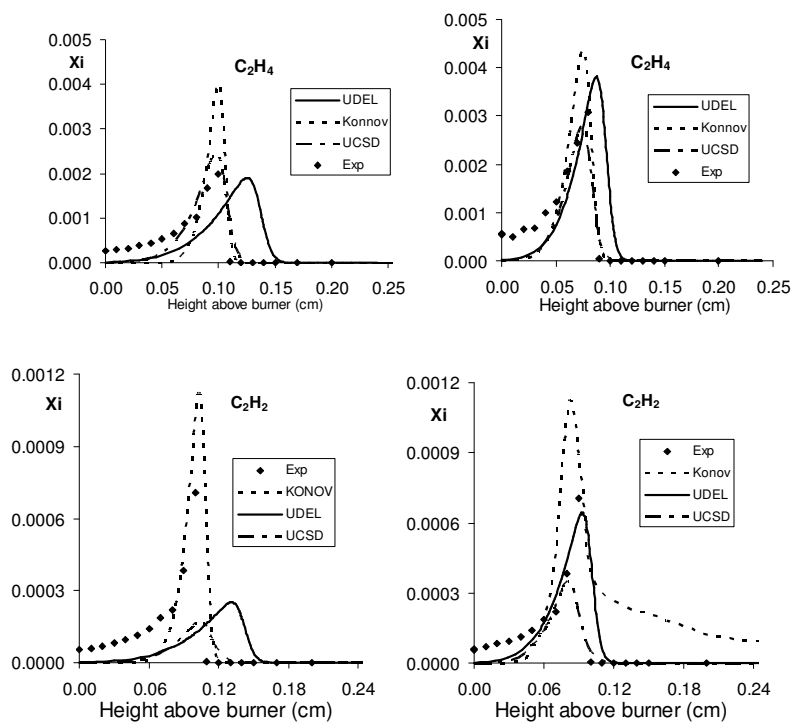
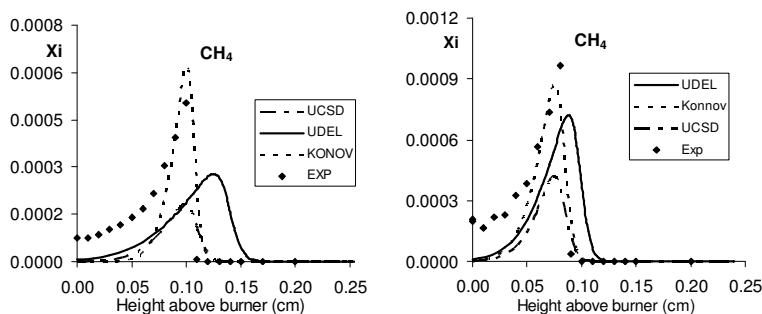


Figure 5. Computed (lines) and measured (symbols) for intermediate species of small hydrocarbon profiles in lean ( $\Phi = 0.48$ , left;  $\Phi = 0.83$ , right) propene flames.



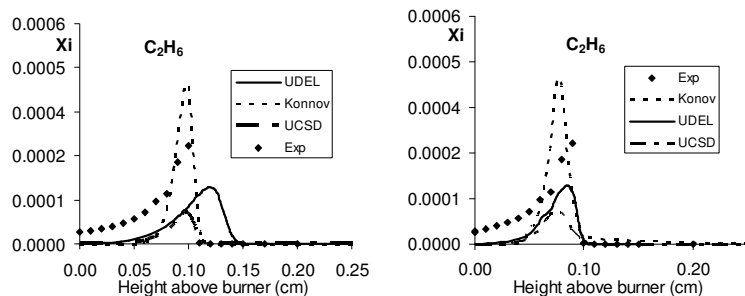


Figure 6. Computed (lines) and measured (symbols) for formaldehyde and acetaldehyde profiles in lean ( $\Phi = 0.48$ , left;  $\Phi = 0.83$ , right) propene flames.

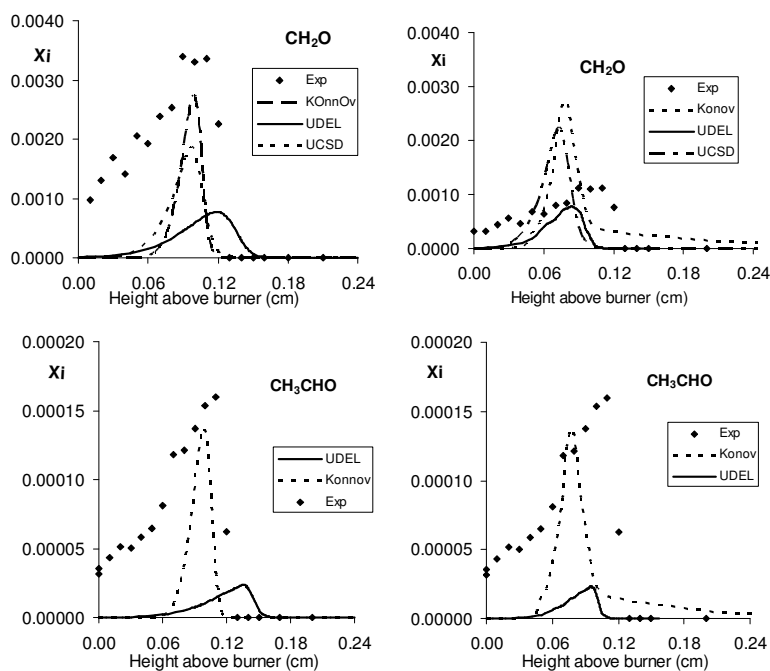


Figure 7. Reaction pathways in C<sub>3</sub>H<sub>6</sub>-O<sub>2</sub>-N<sub>2</sub> flame. Equivalence ratio 0.48 (Konnov mechanism).

As potential pollutants eventually present in the exhaust practical devices using lean combustion, oxygenated intermediate species must be considered carefully. Ketene stability in the sampling line did not allow detecting these species in the chromatograms. Neither methanol nor acrolein could be detected, even in the leanest flame. These species should be analysed on the first gas chromatograph with detection limit estimated to 100 ppm, so that it can be concluded that the maximum mole fraction is smaller than this value for both species. Maximum mole fractions computed by the models were  $6.0 \times 10^{-5}$  (Konnov),  $2.1 \times 10^{-4}$

(UDEL), and  $8.6 \times 10^{-4}$  (UCSD) for methanol. Acrolein is involved only in the UDEL mechanism and its computed maximum mole fraction is  $6.1 \times 10^{-5}$ . Formaldehyde and acetaldehyde were present in the four flames studied. For the former, the maximum mole fraction is under predicted by both mechanisms in the  $\Phi = 0.48$  flame, whereas Konnov and UCSD mechanisms over predict in the  $\Phi = 0.83$  flame by factors equal to 3.

Acetaldehyde is under predicted by Konnov and UDEL in the leanest flame, but, in the richest flame it is under predicted by UDEL, whereas Konnov reproduced fairly well the maximum mole fraction.

The comparisons between computed and measured profiles show that the three mechanisms reproduce very well the main properties of the lean flames: temperature, reactants consumption and main products formation. This comment can be extended to the evolution of the main intermediates: CO, and  $H_2$ . However, we observe divergences between models and experimental data of these intermediates, especially, the minor intermediates than the reactants and products. These comparisons of intermediate species show that any mechanism is presently able to simulate correctly and perfectly the lean propene flame structure. On the other hand, the discrepancies observed for active intermediate species present in low concentration must be related to differences either in the nature of the main reaction pathways or in their relative importance.

To identify in each mechanism the main steps involved in the conversion of the fuel molecule into intermediate and final species, molar fluxes were calculated by integration of local reaction rates over the computation domain:

$$F_k = \int_{z=0}^{z=l} R_k(z) dz \quad (3)$$

where  $R_k(z)$  is local reaction rate of reaction  $k$  ( $\text{mole} \cdot \text{cm}^{-3} \cdot \text{s}^{-1}$ ).

To make easier the comparison of the relative importance of reaction pathways in flames with different equivalence ratios, a fractional carbon conversion flux, expressed as percent of the overall fuel carbon consumption flux was calculated:

$$P_{k,i} = \frac{nC_i F_{k,i}}{3F_{c,C3H6}} \times 100 \quad (4)$$

where  $nC_i$  is the number of carbon atoms in species,  $i$ ,  $F_{ki}$  is the molar flux of formation or consumption of species  $i$  in reaction  $k$ ,  $F_{c,C3H6}$  is the overall molar consumption flux of propene computed as

$$F_{c,C3H6} = \sum_{k=1}^{N_{r,c,C3H6}} F_{k,c,C3H6}, \quad (5)$$

where,  $N_{r,c,C3H6}$  is the number of reactions involved in the fuel consumption.

Figures 8-10 compare the main propene consumption route in the leanest ( $\Phi = 0.48$ ) flame simulated with the three reaction mechanisms. Arrows thicknesses in these curves are proportional to the fractional carbon conversion fluxes. Black arrows correspond to reactions involving non-oxygenated species, dotted arrows to reactions forming oxygenated species with more than one carbon atom, and grey arrows to reactions leading to  $C_1$  oxygenated species, essentially  $CH_2OH$ ,  $CH_2O$ ,  $HCO$ , and  $CO_2$ . This distinction between oxidation and pyrolysis reactions was expected to make more apparent eventual differences between the three mechanisms and, for each mechanism, the influence of the equivalence ratio. Only small

variations are noticed in other flames and the main differences identified from these schemes are common to both flames.

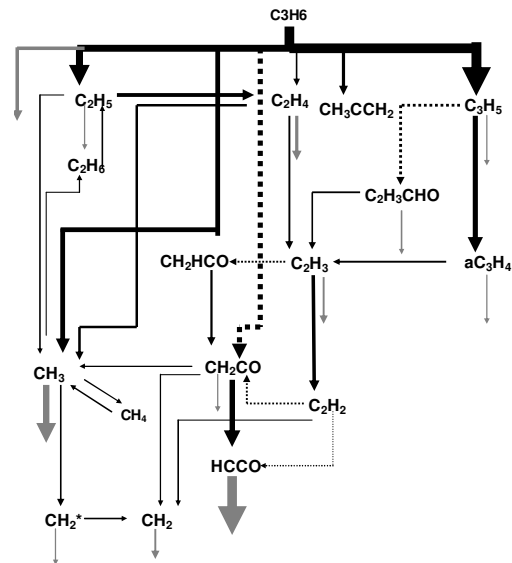


Figure 8. Reaction pathways in C<sub>3</sub>H<sub>6</sub>-O<sub>2</sub>-N<sub>2</sub> flame. Equivalence ratio 0.48 (UDEL mechanism).

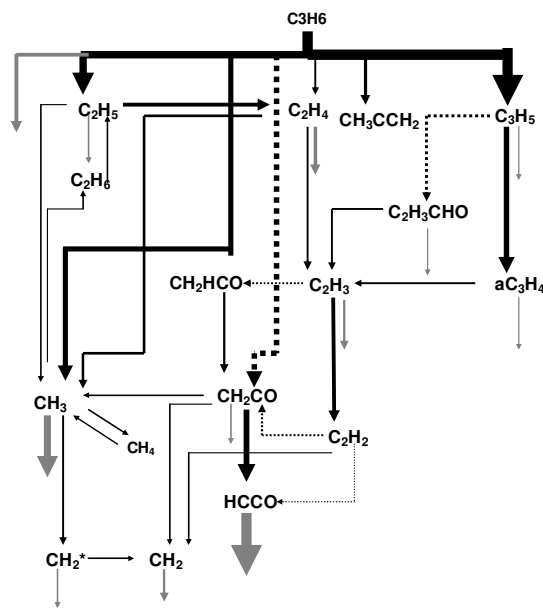


Figure 9. Reaction pathways in C<sub>3</sub>H<sub>6</sub>-O<sub>2</sub>-N<sub>2</sub> flame Equivalence ratio 0.48 (UCSD mechanism).

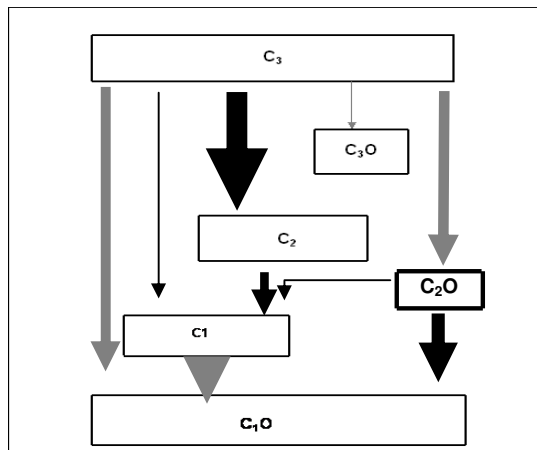


Figure 10. Synthetic reaction pathways in a  $C_3H_6-O_2-N_2$  flame. Equivalence ratio 0.48 (UDEL mechanism).

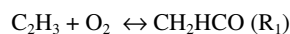
For clarity purpose, the consumption paths are split into three parts: (i) the first steps is the fuel consumption, (ii) and (iii) the consumption of the main intermediates formed in (i): ethyl, ethylene, allyl radical, respectively.

The consumption of propene leads either to  $C_3$  intermediates by reaction with H forming the allyl radical or to  $C_2$  species by addition of O or OH on the double bond followed by a rapid adduct decomposition into  $C_2H_4 + CH_2O$  or  $C_2H_3 + CH_2O$  and with H addition followed by decomposition into  $C_2H_4$  and  $CH_3$ . The oxidation of propene can also proceed to oxygenated species with two carbon atoms in Konnov and UDEL mechanisms. The importance of the two main routes changes markedly from one mechanism to another. Differences in the rate constants in the mechanisms are responsible for these variations.

The allyl radical initiates a  $C_3$  route that either progresses through successive hydrogen loss steps up to  $C_3H_4$  or leads rapidly through  $C_3H_4$  decomposition to  $C_2H_4$ ,  $C_2H_3$ ,  $C_2H_2$  in UDEL mechanisms. Ethyl radical leads essentially to  $C_2H_4$  and  $CH_3$  by decomposition and formation of oxygenated species with two carbon atoms in Konnov mechanism, this reaction is markedly pronounced in UCSD mechanism. The consumption of  $C_2H_4$  involves  $C_2H_3$  and  $C_2H_2$  as intermediate species, but also through reaction with O leading to the formation of  $CH_3$  and HCO. The oxidation of  $C_2H_4$  and  $C_2H_3$  can also proceed without decomposition and initiates the formation of oxygenated species with two carbon atoms in Konnov and mechanisms, 8% and 11%, respectively. On the other hand, the consumption of  $C_2H_4$  by H atom abstraction to  $C_2H_3$  is 19%, 7%, and 24% for UCSD, UDEL, and Konnov mechanisms, respectively. In the lean flames studied in this work, methyl radicals are consumed by reactions with O,  $HO_2$ , and OH. The formers give rise to oxygenated species  $CH_2O$  and  $CH_3O$ , whereas the latter forms  $CH_2$  radicals. As a result, the overall fuel carbon conversion through  $C_2H_4$  formation is closely similar with Konnov and UCSD mechanisms.

A more careful examination shows that differences are noticeable at various stages of the schemes. For very first steps of propene consumption, the Konnov, UCSD, and UDEL mechanisms predict that the formation of  $C_3H_5$  represents 29%, 27%, and 32%, respectively, in terms of conversion, whereas the formation of ethyl radical is 23%, 35%, and 8% for Konnov, UCSD, and UDEL, respectively.

The similarities between Konnov and UCSD mechanisms is no longer sustained at the next step because the direct formation of CH<sub>3</sub>O radical (13%) from propene in Konnov mechanism. The fraction of ethylene molecule converted into C<sub>2</sub>H<sub>3</sub> or CH<sub>2</sub>HCO also changes markedly from one mechanism to another. Expressed as ratios  $P_{f,C_2H_3}/P_{f,CH_2HCO}$  the relative importance of the vinyl and vinoxy radical is: 3.7 (Konnov), 1.01 (UDEL), and 1.69 (UCSD). The vinyl radical consumption differs markedly with Konnov mechanism compare to the two others mechanisms. The formation of acetylene by H atom abstraction is dominant so that this specie contributes to the ethylene carbon atom conversion by 12%. Values obtained by the others mechanisms are considerably smaller: 3% (UDEL) and 4% (UCSD). However, as amongst the various consumption of the vinyl radical, the reaction with O<sub>2</sub> forms the vinoxy radicals; its contribution to the carbon conversion must be removed to C<sub>2</sub>H<sub>3</sub> and added to CH<sub>2</sub>HCO:



Other reaction relative to a consumption of vinyl radical is the formation of CH<sub>2</sub>O and HCO:



The relative importance of these two routes R<sub>1</sub>/R<sub>2</sub> is: 0.74 (UDEL), 1.88 (Konnov), and 3.87 (UCSD). Other differences concern the formation paths of CH<sub>2</sub>CO and the role played by this radical in the formation of C<sub>1</sub> oxygenated species. In term of fuel carbon atom conversion, this latter corresponds to 7.5% (Konnov), 2.58% (UDEL), and 13.71 (UCSD). The direct formation of C<sub>1</sub> oxygenated species from propene is also markedly different. It represents: 24.3%, 3.9%, 12.72% fuel carbon atom conversion for the UCSD, UDEL, and Konnov mechanisms, respectively. Indeed, the formation of ketene is common to the three mechanisms but its contribution to the consumption of the vinoxy radical varies markedly. It is the unique vinoxy consumption path in UCSD mechanism by 30% in terms of the carbon atom conversion, it occurs dominantly in the UDEL mechanism whereas it is only a secondary path in Konnov mechanism where CH<sub>3</sub>CO is the main intermediate.

To simplify the reaction path schemes, species with the same number of carbon atoms were grouped into classes, with a distinction made between oxygenated and non-oxygenated species so that the classes included C<sub>3</sub>, C<sub>3</sub>O, C<sub>2</sub>, C<sub>2</sub>O, C<sub>1</sub>, and C<sub>1</sub>O. Overall percentage fuel carbon conversions were computed by summing the contributions of individual reactions converting species of one class into another class. Skeleton graphs so obtained have been drawn in Figures 11 and 12 with black arrows for reactions that do not involve oxygen addition to hydrocarbons and grey arrows for oxidation reactions.

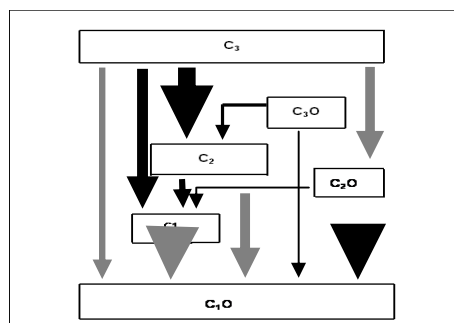


Figure 11. Synthetic reaction pathways in a C<sub>3</sub>H<sub>6</sub>-O<sub>2</sub>-N<sub>2</sub> flame. Equivalence ratio 0.48 (UCSD mechanism).

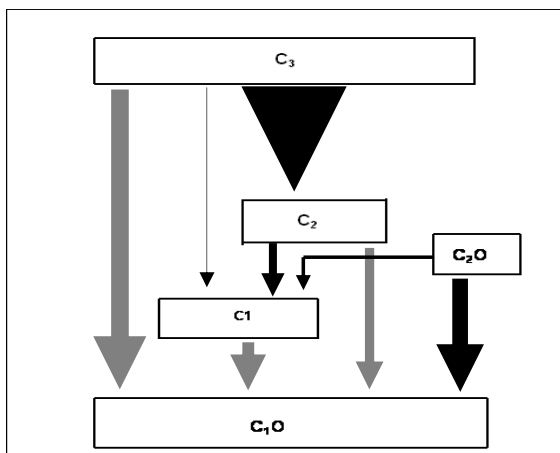


Figure 12. Synthetic reaction pathways in a  $C_3H_6-O_2-N_2$  flame. Equivalence ratio 0.48 (Konnov mechanism).

Except for the direct formation of  $C_3O$  species from  $C_3$  species with the former, the UCSD and Konnov mechanisms exhibit closely similar synthetic reaction paths. Expressed in term of percentage fuel carbon atom conversion, the formation of  $C_2$ ,  $C_1$ , and  $C_1O$  species contributes: 38.02%, 1.15%, and 16.04% to the conversion of  $C_3$  species with Konnov mechanism and 64.14%, 3.66%, 32.3% with UCSD mechanism. The consumption of  $C_2$  species occurs essentially through oxidation leading to  $C_2O$  species. Marked differences are observed with UDEL mechanism.

The direct formation of  $C_2O$  species contributes significantly to the consumption of  $C_3$  species (20.82%) in addition to  $C_2$  (41.7%) and  $C_1$  (20.32%) routes and a very minor  $C_1O$  (10.68%) route. Another difference concerns the consumption of  $C_2$  species that leads predominantly to the formation of  $C_1O$ .

## CONCLUSIONS

The structure of lean, premixed propene-oxygen-nitrogen stabilized at atmospheric pressure was studied both experimentally and numerically. Three mechanisms were used for the simulations. Data obtained were used to check ability of three detailed mechanisms to correctly predict the temperature and species mole fraction profiles. Despite large differences in their number of species and reactions, the very good agreement observed for the reactants consumption and the final products formation constitutes a minimum requisite since in very lean flames  $CO_2$  and  $H_2O$  are the only final products corresponding to the complete conversion of C and H, respectively. On the other hand, differences between the mechanisms were observed when the prediction of the mole fraction profiles of the active intermediate species was considered.

Pathways analyses helped identifying the main causes of these differences. It shows that the fuel consumption routes are essentially similar with the three mechanisms. However, a more detailed examination exhibits some differences in the relative importance of  $C_3$ ,  $C_2$ , and  $C_1$  channels in the role played by  $C_2O$  species.  $C_2H_5$ ,  $C_2H_4$ , and  $C_3H_5$  are the main species formed in the first step and their consumption increases the differences between the mechanisms either by the use of different kinetic data for common reactions or by differences in the nature of the consumption reactions.

## ACKNOWLEDGEMENTS

Financial supports from the Region Centre (J. Biet grant) and from EGIDE (A. Seydi fellowship) are greatly appreciated.

## REFERENCES

1. Frimstom, R.M.; Avery, W.H.; Grunfelder, C. *Proc. Combust. Int.* **1959**, 7, 304.
2. Mahnen, G. *Thèse de Doctorat*, Université Catholique de Louvain, Belgique, **1973**.
3. Biord, J.C.; Lagara, C.P.; Papp, J.F. *Proc. Combust. Int.* **1976**, 16, 1097.
4. Bhargava, A.; Westmoreland, P.R. *Combust. flame* **1998**, 115, 456.
5. Balvarens, B.; Vandooren, J.; Van Tiggelen, J.P. *Combust. Sci. Technol.* **1999**, 130, 399.
6. Crunelle, B.; Surdyk, D.; Pauwells, J.F.; Sochet, L.R. *J. Chim. Phys.* **1997**, 94, 433.
7. Gasnot, L.; Degroux, P.; Pauwells, J.F.; Sochet, L.R. *Combust. Flame* **1999**, 117, 291.
8. Thomsen, D.D.; Kuligowsky, F.; MLaurendeau, N. *Combust. Flame* **1999**, 119, 307.
9. Reisel, J.R.; Carter, C.D.; Laurendeau, N.M. *Energy Fuels* **1999**, 11, 1092.
10. Kaiser, E.W.; Wallington, T.J.; Hurley, M.D.; Platz, J.; Curran, H.; Pitz, J.W.; Westbrook, J.C.K. *J. Phys. Chem.* **2000**, 104, 8194.
11. Kaiser, E.W.; Rostchild, W.G.; Lavoie, G.A. *Combust. Sci. Technol.* **1984**, 41, 271.
12. Warnatz, J. *Proc. Combust. Inst.* **1984**, 20, 845.
13. Biet, J.; Delfau, J.L.; Seydi, A.; Vovelle, C. *Combust. Flame* **2005**, 142, 197;  
Biet, J. *Thèse de Doctorat*, Université d'Orléans, France, **2004**.
14. Delfau, J.L.; Biet, J.; Idir, M.; Pillier, L.; Vovelle, C. *Proc. Combust. Inst.* **2007**, 31, 317.
15. Dagaut, P.; Cathonet, M.; Boetner, J.C. *Combust. Sci. Technol.* **1992**, 83, 167.
16. Thomas, S.D.; Bhargava, A.; Westmoreland, P.R.; Lindsted, R.; Skevis, G. *Bull. Soc. Belg.* **1996**, 105, 501.
17. Davis, S.G.; Law, C.K.; Wang, H. *Combust. Flame* **1999**, 119, 375.
18. Burcat, A.; Radhakrishnan, K. *Combust. Flame* **1985**, 60, 157.
19. Qin, Z.W.; Yang, H.X.; Gardiner, W.C.J. *Combust. Flame* **2001**, 124, 246.
20. Heyberger, B.; Benekki, N.; Courand, V.; Glaude, P.A.; Fournet, R.; Battin-Clerc, F. *Int. J. Chem. Kinet.* **2002**, 34, 666.
21. Zheng, L.; Kazakov, A.; Dryer, F.L. *Proceedings of the Third Joint Meeting of the US Sections of the Combustion Institute*, A03, **2003**.
22. Baldwin, R.R.; Dean, C.E.; Walker, R.W.J. *Chem. Soc. Farad. Trans. II* **1986**, 82, 1445.
23. Baldwin, R.R.; Hisham, M.W.M.; Walker, R.W. *Twentieth Symposium (International) on Combustion*, The Combustion Institute: Pittsburg; **1984**; p 743.
24. Wilk, R.D.; Cernansky, N.P.; Cohen, R.S. *Combust. Sci. Technol.* **1987**, 52, 39.
25. Lignola, P.G.; Reverchon, E.R.; Autuori, R.; Insoia, A.; Siverstre, A.M. *Combust. Sci. Technol.* **1985**, 1, 44.
26. Bawn, C.E.H.; Skirrow, G. *Fifth Symposium (International) on Combustion*, The Combustion Institute: Pittsburg; **1955**; p 521.
27. Mullen, J.D. Skirrow, G. *Proc. R. Soc. Lond. A* **1958**, 224, 312.
28. Baldwin, R.R.; Walker, R.W. *Eighteenth Symposium (International) on Combustion*, The Combustion Institute: Pittsburg; **1981**; p 819.
29. Westbrook, C.K.; Pitz, W.J. *Combust. Sci. Technol.* **1984**, 3, 117.
30. Dagaut, P.; Luche, J.; Cathonet, M. *Combust. Flame* **2000**, 121, 555.
31. Pope, C.J.; Miller, J.A. *Proc. Combust. Inst.* **2000**, 28, 1519.
32. Koshe-Höinghauss, K.; Osswald, P.; Struckmeier, U.; Kasper, T.S.; Hansen, N.; Taatjes, C.A.; Wang, J.; Cool, T.A.; Gon, S.; Westmoreland, P.R. *Proc. Combust. Inst* **2007**, 31, 1119.

33. Wang, J.; Struckmeier, U.; Cool, T.A.; Bwald, P.; Koshe-Höinghauss, K.; Kasper, T.S.; Hansen, N.; Westmoreland, P.R. *J. Phys. Chem. A* **2008**, 112, 9255.
34. Cong, T.L.; Bedjanian, E.; Dagaut, P. *Combust. Sci. Technol.* **2010**, 182, 333.
35. Frassoldati, A.; Faravelli, T.; Koshe-Höinghauss, K.; Westmoreland, P.R. *Combust. Flame* **2011**, 158, 1264.
36. Qin, Z.; Lissianski, V.V.; Yang, H.; Gardiner, W.C.; Davis, S.G.; Wang, H. *Proc. Combust. Inst.* **2000**, 28, 1663.
37. Konnov, A.A. *Proc. Combust. Inst.* **2000**, 28, 317.
38. Williams, F.A.; University of California, San Diego, Center for Energy Research, Combustion Division; available at: <http://macmail.ucsd.edu/Combustion/cermech/> accessed in **2002**.
39. Vovelle, C.; Foulatier, R.; Delbourgo, R. *Méthodes Phys. Anal.* **1974**, 7, 353.
40. Kent, J.H. *Combust. Flame* **1970**, 14, 279.
41. Bonne, U.; Grever, Th.; Wagner, H. Gg. *Z. Phys. Chem.* **1960**, 26, 93.
42. Kee, R.J.; Rupley, F.M.; Miller, J.A. *Chemkin-II: A Fortran Chemical Kinetics Package for the analysis of Gase Phase Chemical Kinetics, Sandia Reports SAN89-8009B*, **1989**.
43. Kee, R.K.; Gear, F.; Smooker, M.D.; Miller, J.A. *A Fortran Program for Modeling Steady Laminar One- Dimensional Premixed Flames, Sandia Technical Report SAND85-8240*, **1985**.
44. Smith, G.P.; Golden, D.M.; Frenklack, M. Available at <http://www.berkerley.edu/grimech/> accessed in **1998**.
45. Renard, C.; Van Tiggelen, P.J.; Vandooren, J. *Proc. Eur. Combust. Meeting*, **2005**, # 017, 92.